Int. J. Electrochem. Sci., 11 **(2016)** 9192 – 9205, doi: 10.20964/2016.11.04

International Journal of ELECTROCHEMICAL SCIENCE
www.electrochemsci.org

Corrosion Protection of AISI 316L Stainless Steel with the Sol-Gel Yttria Stabilized ZrO_2 Films: Effects of Sintering Temperature and Doping

Ivana Bačić[1], Helena Otmačić Ćurković[2], Lidija Ćurković[3,], Vilko Mandić[4], Zrinka Šokčević[3]*

[1] Forensic Science Centre ''Ivan Vučetić'', 10000 Zagreb, Croatia,
[2] Faculty of Chemical Engineering and Technology, 10000 Zagreb, Croatia
[3] Faculty of Mechanical Engineering and Naval Architecture, 10000 Zagreb, Croatia
[4] Ruđjer Bošković Institute, Bijenička cesta 54, 10000 Zagreb, Croatia
[*]E-mail: lidija.curkovic@fsb.hr

Received: 29 July 2016 / *Accepted:* 27 August 2016 / *Published:* 10 October 2016

Nanostructured sol–gel zirconia (ZrO_2) films containing 3, 5 and 7 mol % Y_2O_3 of one and three layers were prepared on stainless steel X2CrNiMo17-12-2 (AISI 316L) surface by the dip coating method. Yttria stabilized zirconia (YSZ) deposited films were sintered at 400 and 600 °C. For the preparation of sol zirconium(IV) butoxide was used as precursor, *i*-propyl alcohol as a solvent with addition of nitric acid as a catalyst, acetylacetone as chelating agent and water for hydrolysis. Thickness of sol-gel YSZ films deposited on stainless steel was determined by glow-discharge optical emission spectrometry (GD-OES). It was found that thickness of deposited films is barely affected by yttria content while increases by increasing the number of layers and temperature of sintering. The crystal structure of films was determined by X-ray diffraction. The corrosion resistances of uncoated and coated specimens were studied by electrochemical impedance spectroscopy (EIS) and potentiodynamic polarization in simulated marine environment (3.5 *wt.* % NaCl aqueous solution) at room temperature. The influence of yttria stabilized zirconia (YSZ) layers number and temperature of sintering on the corrosion protection was examined as well. Sol-gel derived YSZ films are capable of appreciable improvement in corrosion resistance of stainless steel in the investigated corrosive medium.

Keywords: sol-gel, ZrO_2 films, GD-OES, electrochemical techniques

1. INTRODUCTION

In spite of much advancement in the science and technology of corrosion prevention and control, the phenomenon of corrosion (usually of metals and alloys) continues to pose a major concern

to many industries around the world. The direct and indirect cost of corrosion is huge and a good portion of the loss can be avoided by proper corrosion control and monitoring. In general, corrosion can be prevented by suitable modifications in: material (e.g. selection of corrosion resistant materials), environment (e.g. addition of inhibitors) and material surfaces (e.g. coatings, films). Due to its properties, stainless steels are common construction materials with applications in various industries, and are an excellent choice when good corrosion resistance is required. Corrosion resistance of stainless steels is associated with the formation of a thin passive film on the alloy surface [1]. However, the stability of the natural protective layer of chromium oxide (Cr_2O_3) may be violated in aggressive chloride environment like the marine environment, which can result in the development of localized pitting corrosion and irreversible damage to the steel product [2]. Corrosion resistance of stainless steels in the presence of chloride ions can be improved by application of protective coatings or corrosion inhibitors. Besides, in order to improve the corrosion resistance of stainless steel and extend their durability, the systematic research has been conducted with the aim to improve existing or develop new ways of surface protection, especially those based on the application of thin films and nanotechnology [3]. Materials (thin films) obtained by nanotechnology is one of the newer trends in the prevention of corrosion, primarily due to unique and generally improved properties in relation to traditionally prepared materials [4]. Therefore, various surface modification techniques were developed to improve metals and alloys corrosion properties. Some commonly used surface modification techniques are chemical vapor deposition (CVD) [5, 6], physical vapor deposition (PVD) [7], ion implantation [8], electrodeposition [9, 10], plasma [11], sol–gel process [12-15], etc. The reasons behind the widespread exploitation of sol–gel coatings are following [3]: (*i*) sol–gel coatings can be produced with compositions that are not obtainable by other means, (*ii*) sol–gel enables integrated multilayering at a lower cost than vacuum techniques, (*iii*) sol–gel can be easily combined with other methods of coating synthesis and coating application processes to put down coatings on substrates from sol-gel solution, (*iv*) processing temperature of sol–gel coatings generally is low, frequently close to room temperature which is environmentally and economically more acceptable, (*v*) sol–gel coatings are formed by "green" coating technologies, it uses compounds that do not introduce impurities into the end product as initial substances, this method is waste-free and excludes the stage of washing, (*vi*) sol–gel processes can be used to form nanostructured films (typically 200 nm to 10 μm in overall thickness) that are more resistant than metals to oxidation, corrosion erosion and wear.

Today, sol–gel based coatings are being used in every sector of engineering application, such as aerospace, electronics, ships, building, decorative, etc. However, development and industrialization of sol–gel coatings are still in the initial stages.

Many nanostructured sol-gel ceramic films and coatings like ZrO_2 [16], TiO_2 [15, 17], ZrO_2-TiO_2 [18], Al_2O_3 – yttria stabilized ZrO_2 [19, 20], SiO_2 [21], SiO_2 -TiO_2 - ZrO_2 [22] etc. can be deposited on metals and alloys to significantly improve their corrosion resistance in aggressive media.

In this paper, in order to improve corrosion behavior of stainless steel X2CrNiMo17-12-2 (AISI 316L), nanostructured yttria stabilized ZrO_2 films were deposited on the steel surface by dip-coating sol–gel method. Effects of different amount of yttrium acetate for the stabilization of crystal structure, number of layers and sintering temperature on corrosion properties of the ZrO_2 thin film

were investigated. Corrosion resistance of protected and unprotected stainless steel were examined in 3.5 *wt.* % NaCl aqueous solution by electrochemical methods.

2. MATERIALS AND METHODS

2.1. Deposition of sol-gel ZrO_2 films on stainless steel

Steel disks with diameter 16 mm and height 2 mm were used as substrates. Chemical composition of X2CrNiMo17-12-2 (AISI 316L) stainless steel was determined by glow discharge optical emission spectroscopy (GDS 850A, Leco) and results in *wt.* % are: C-0.026; P-0.0287; S-0.0021; Si-0.37; Mn-1.42; Cu-0.345; Mo-2.17; Cr-16.38; Ni-10.53 and Fe – balance. Before the deposition of films, steel substrates were ground with SiC abrasive discs (180–1000 grit) and then polished with diamond paste (3 μm and 0.25 μm). Substrates were then ultrasonically cleaned in acetone and subsequently dried prior to the deposition process.

For the preparation of sol zirconium(IV) butoxide (ZrB) was used as precursors, *i*-propyl alcohol (*i*-PrOH) as a solvent, acetylacetone (AcAc) as chelating agent, with addition of nitric acid as a catalyst, and yttrium acetate hydrate (YAc) was used for ZrO_2 stabilization.

Three sols were prepared, the molar ratio of the reagents in all sols was: ZrB:*i*-PrOH:AcAc:HNO_3=1:18:0.7:0.002, respectively. Sol 1 contained 3 mol % Y_2O_3 (3YSZ), sol 2 contained 5 mol % Y_2O_3 (5YSZ), and sol 3 contained 7 mol % Y_2O_3 (7YSZ). The appropriate quantity for a final composition of 3, 5 and 7 mol % Y_2O_3 to ZrO_2 was calculated and used.

After 24 h aging, the stainless steel disks were dipped once and three times into sol 1 (for deposition 3YSZ film), sol 2 (for deposition 5YSZ film) and sol 3 (for deposition 7YSZ film) by an in-house developed, electrically driven pulley system. Steel substrates were dipped into sol at a rate of 30 mm/min, then were held in solution for 3 minutes, in order to allow surface wetting. The withdrawal rate was also 30 mm/min. The steel substrates were then dried at room temperature for 30 minutes. After drying at room temperature, each steel substrate was dried at 100 °C for an hour. The same procedure followed after each dip, for steel substrates which were dipped three times for deposition three layers TiO_2 films. After dip coating and drying, steel substrates were calcined at 400 °C and 600 °C for 1 hour.

2.2. Characterization of sol-gel ZrO_2 films on stainless steel

In this study, glow discharge optical emission spectrometry (GD-OES), Leco GDS-850A spectrometer, equipped with a Grimm-type DC lamp for conductive samples was used for analysis of stainless steel substrate as well as for quantitative depth profiling (QDP) and the thickness of films of sol-gel ZrO_2 films deposited on stainless steel. The anode has a diameter of 4 mm, for a sampling area of 12.5 mm^2. The spectrometer is equipped with dual Rowland circles, having curved, holographic diffraction gratings of 1800 lines/mm and 3600 lines/mm, respectively, for a spectral range of 120–800 nm.

The crystal phases in calcined bulk powder samples were identified by powder X-ray diffraction (PXRD) using Shimadzu diffractometer XRD6000 with CuKα radiation. Data were collected 5–70°2θ in a step scan mode with steps of 0.02° and counting time of 0.6 s under accelerating voltage of 40 kV and 30 mA current.

2.3. Electrochemical measurements

Electrochemical measurements, i.e. electrochemical impedance spectroscopy (EIS) and potentiodynamic polarization were conducted in a conventional three electrode cell. Saturated calomel electrode (SCE) was used as a reference and platinum plate as the counter electrode. Working electrode was stainless steel disc covered by ceramic coating and inserted in Teflon electrode holder, such that exposed area was 1 cm^2.

Studies were performed in simulated marine environment in near neutral 3.5 *wt.* % aqueous NaCl solution. Solutions were prepared from p.a. grade chemicals and bidistilled water.

Electrochemical impedance spectroscopy (EIS) measurements were conducted after 1 h immersion in corrosive medium. This was sufficient period of time for open circuit potential (E_{oc}) to reach stable value. Measurements were performed in the frequency range from 100 kHz to 0.01 Hz. The amplitude of the voltage perturbation was 0.01 V_{rms}. All experiments were performed at open circuit potential.

Potentiodynamic polarization was conducted from E = -250 mV vs. E_{oc} to 200 mV vs. E_{oc} with a scan rate 0.166 mV s^{-1}. Measurements were performed using PAR 263A potentiostat/galvanostat and Frequency response analyser 1025.

3. RESULTS AND DISCUSSION

Thickness of sol-gel ZrO_2 films deposited on stainless steel was determined by glow-discharge optical emission spectrometry (GD-OES). Figures 1 and 2 show GD-OES depth profiles of Zr, Cr, Ni and Fe (at.% as a function of depth) for the sol-gel ZrO_2 films with 1 layer and 3 layers obtained from sol 2 (5YSZ films) and heated at 400 and 600 ºC, respectively (Figures of quantitative depth profile analysis of sol-gel ZrO_2 film obtained from sol 1: 3YSZ films and sol 3: 7YSZ films are not shown here).

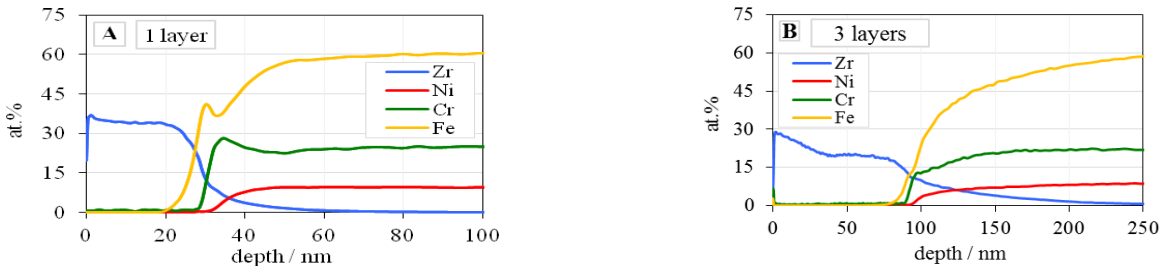

Figure 1. Quantitative depth profile analysis of sol-gel ZrO_2 films obtained from sol 2 (5YSZ films) with (A) 1 layer and (B) 3 layers on stainless steel obtained by GD-OES, heat-treated at 400 ºC for 60 min.

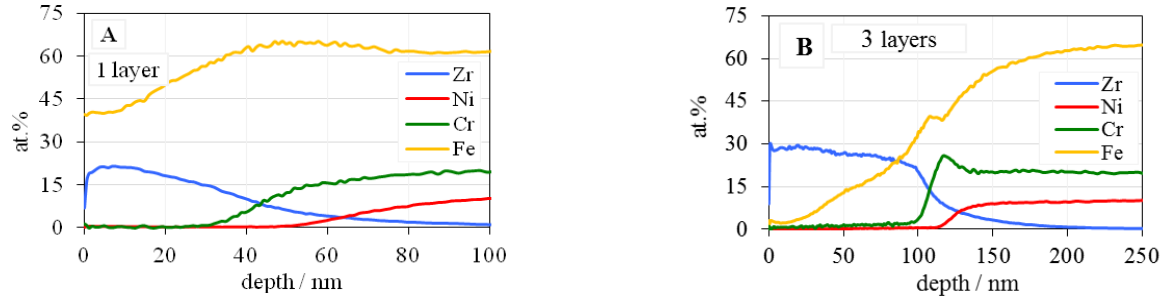

Figure 2. Quantitative depth profile analysis of sol-gel ZrO_2 films obtained from sol 2 (5YSZ films) with (A) 1 layer and (B) 3 layers on stainless steel obtained by GD-OES, heat-treated at 600 ºC for 60 min.

The film thickness was estimated from the zirconium depth profile considering the range where at.% of Zr begins to decrease and signal of first detected substrate element (Fe or Cr) achieves significant value. Results of GD-OES thickness measurements of all investigated sol-gel ZrO_2 films obtained from sol 1 (3YSZ film), sol 2 (5YSZ film) and 3 sol (7YSZ film) are presented in Table 1.

Table 1. Thickness of sol-gel ZrO_2 films obtained by GD-OES analysis.

Sample	Sol, film	*T*, °C	Number of layers	Thickness, nm
ZrO_2 film	sol 1, 3YSZ film	400	1	47
			3	123
		600	1	27
			3	133
	sol 2, 5YSZ film	400	1	28
			3	93
		600	1	43
			3	108
	sol 3, 7YSZ film	400	1	50
			3	115
		600	1	33
			3	130

Results presented in Table 1 show that the thickness of the deposited films increases by increasing the number of deposited layers. The thickness of deposited sol 2 ZrO_2 films (5YSZ films) with 1 layer and 3 layers thermally treated at 400 °C are slightly thinner than sol 1 ZrO_2 films (3YSZ films) and sol 3 ZrO_2 films (7YSZ films) films but not significantly different.

The thickness of films heated at 600 °C is not notably different from those heated at 400 ºC. It was observed that iron diffusion through films heated at 600 °C is not limited to a narrow diffusion layer as in samples heated at 400 °C, but extends almost through the whole profile of the ZrO_2 films.

Bulk powders of samples sol 1 (3YSZ powder), sol 2 (5YSZ powder) and sol 3 (7YSZ powder) thermally treated at 400 and 600 °C were prepared following the same procedure as for the coatings and thereafter characterised structurally using XRD (Figure 3).

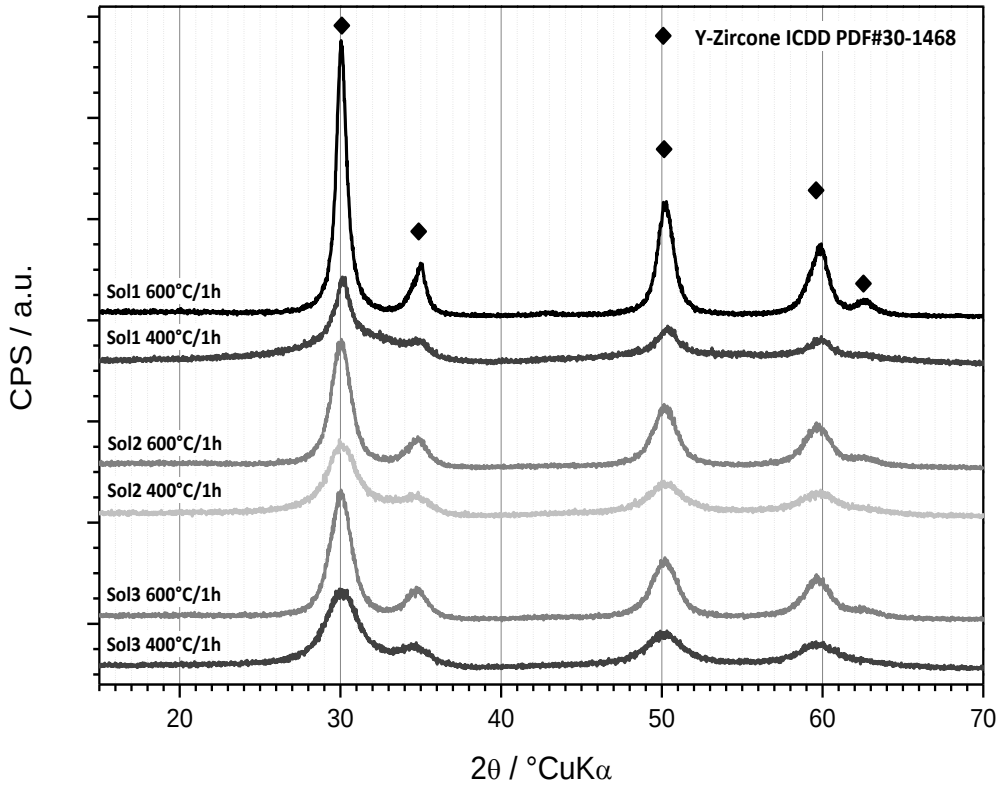

Figure 3. Diffraction patterns of bulk powders for all samples treated at 400 and 600 °C (sol 1: 3YSZ powder, sol 2: 5YSZ powder and sol 3: 7YSZ powder).

All samples exhibit crystalline phase assigned to zirconia (ICDD PDF#30-1468) in cubic structure on behalf of yttira doping. However, determination of structural type of nanocrystalline ZrO_2, based exclusively on the XRD analysis can be very difficult due to high structural similarity of cubic and tetragonal polymorphs. Namely, nanocrystalline character (and stress and defects) of the samples contribute to significant line broadening. This broadening can, having in mind the ZrO_2 polymorphs can be distinguished by vague splitting of lines in tetragonal diffraction pattern, while in cubic diffraction pattern these peaks remain single [23, 24], easily prevent unambiguous distinction between the *t*-ZrO_2 and *c*-ZrO_2 phase. Obviously, doping levels remained appropriate for crystallisation of zirconia in the high-temperature structural form. The width of the diffraction peaks suggest lower temperature of thermal treatment favour nanocrystalline product, as it was calculated from Scherrer's equation for determination of crystallite size (Figure 4). Such behaviour is consistent for sol-gel derived products. Much more interesting is the dependency of crystallite size to the doping level.

However this difference is only minute at 400 °C, and considerable at 600 °C. Probably the higher content of yttrium precursor requires somewhat higher temperatures for full conversion of the gels to product. Thereby crystallisation takes place at somewhat higher temperature and product remains nanocrystalline for longer period. At this point one can presume the lower crystallite size is achieved for the dense yttria stabilised zirconia coatings the better anti-corrosion properties should be displayed, primarily due to diminishing of diffusion through the coating.

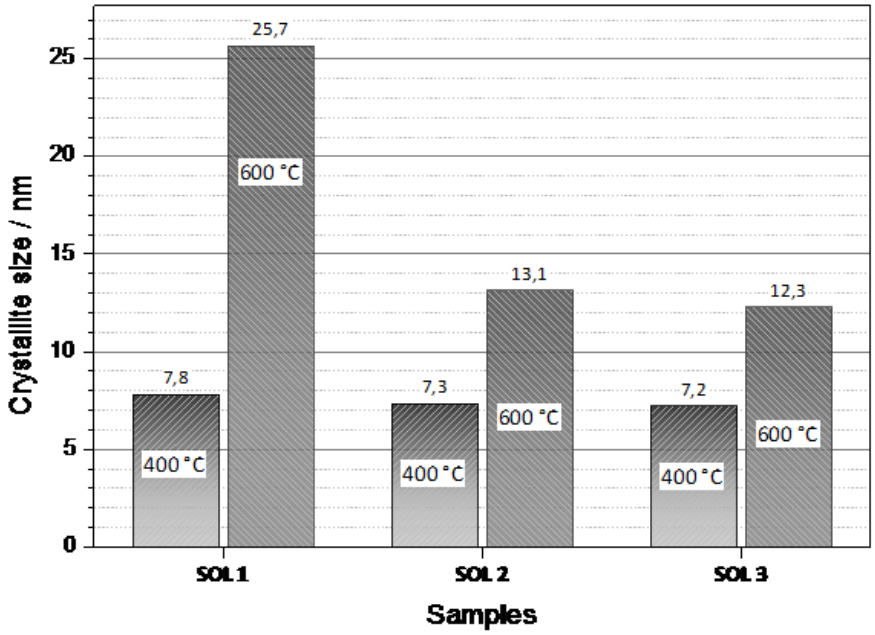

Figure 4. Crystallite sizes for all samples treated at 400 and 600 °C (sol 1: 3YSZ powder, sol 2: 5YSZ powder and sol 3: 7YSZ powder).

Potentiodynamic polarization was conducted in chloride solution on all examined samples. The representative polarization curves for bare stainless steel and protected with 3 layers of ZrO_2 coatings cured at 400 °C are given in Figure 5. It can be seen that coated samples show lower current densities and nobler corrosion potentials than bare steel. The cathodic current densities seem to decrease more significantly than anodic current densities, indicating that coating is an efficient barrier to O_2 diffusion towards steel surface. From the polarization curves corrosion current densities and corrosion potentials were determined (Table 2). For samples covered with any of three sols heated at 400 °C corrosion current density is more than ten times lower than that of the blank sample. Among the coatings with one layer the corrosion current density decreases with the increase of yttrium content.

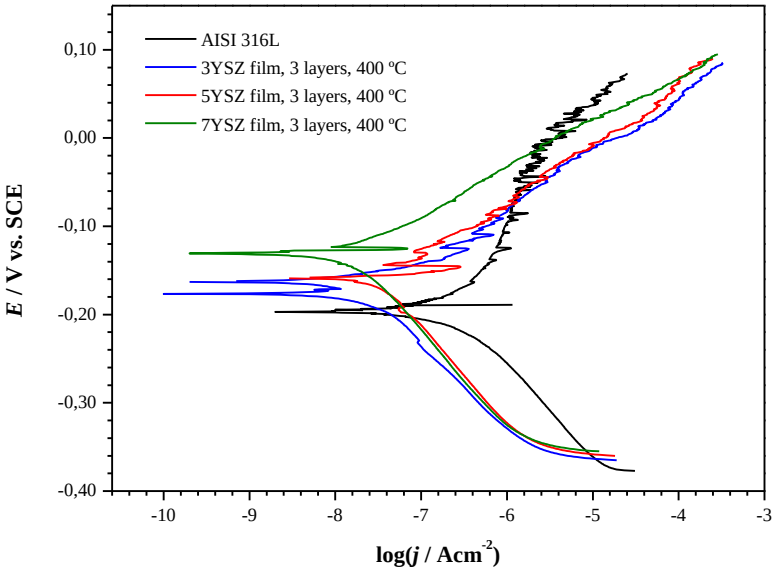

Figure 5. Polarization curves for uncoated AISI 316L stainless steel and coated with ZrO_2 films with different content of Y_2O_3 (sol 1: 3YSZ film, sol 2: 5YSZ film and sol 3: 7YSZ film).

Figure 6 shows polarization curves for samples with 1 and 3 layers of sol 3 (7YSZ films). Thicker coating causes decrease in anodic current densities and shift of the E_{corr} towards more noble values, compared to 1 layer coating. However, the observed decrease in j_{corr} is not proportional to increase in coating thickness but much lower. Similarly is observed for 1 and 3 layer coatings of sol 1 (3YSZ films). It is interesting to notice that for sol 2 one layer coating (5YSZ film) provides slightly better protection than the three layer coating.

While all coatings cured at 400 °C provide corrosion protection to underlying steel substrate, this is not the case for any of the coatings cured at 600 °C. Instead, for these samples the corrosion current density was higher than that of the unprotected stainless steel. Such behaviour can be correlated with GD-OES results (Figure 2) that showed diffusion of Fe through complete ZrO_2 coating, even for three layer structures. Thus, for 1 layer coating, iron can be found in the outer part of the coating in a very high quantity while chromium content is lower than in the substrate alone. On behalf of corrosion of iron in the surface proximity the corrosion currents are the same or higher than the blank sample. The worst results were observed for sol 1 coating (3YSZ film) which exhibits the highest crystallite size and the highest Fe content on the surface (60 at.%).

Three layered coatings, cured at 600 °C, have lower iron content in outer part of the coating compared to one layered coatings but despite of that higher corrosion current densities were obtained. One of the possible reasons could be the formation of bigger number of defects in three layer coatings during the curing process while other possible reason could be related to formation of galvanic couple. Namely, for all sols three layered coatings have lower iron surface content than one layered coatings. Thus the anodic area (Fe) is much smaller than cathodic area (ZrO_2) leading to intensive galvanic corrosion of Fe which reflects in high anodic currents (Figure 6).

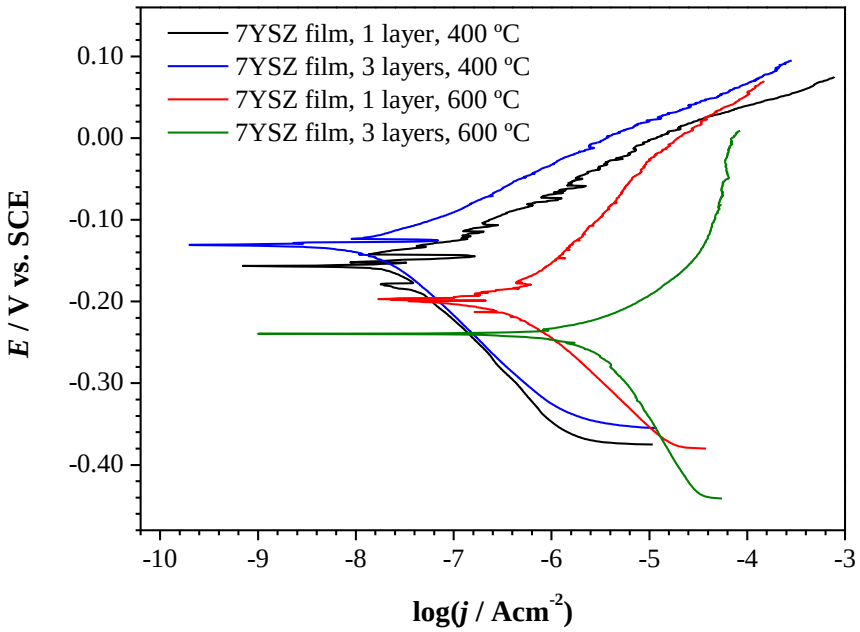

Figure 6. Influence of the heat treatment temperature and coating thickness on polarization curves of stainless steel coated with YSZ film with 7 mol.% of Y_2O_3 (sol 3: 7YSZ films).

Table 2. Values of corrosion potential (E_{oc}) measured in 3.5 *wt*. % aqueous NaCl solution for ZrO_2 films with 1 layer and 3 layers obtained from sol 1 (3YSZ films), sol 2 (5YSZ films) and sol 3 (7YSZ films) heat treated at 400 °C or 600 °C.

Sample	Sol, film	*T*, °C	Number of layers	E_{corr} / V vs. SCE	j_{corr} / μA cm^{-2}
AISI 316L	--	25	--	-0.201	0.405
ZrO_2 film	sol 1, 3YSZ film	400	1	-0.192	0.038
			3	-0.175	0.028
		600	1	-0.202	2.801
			3	-0.259	3.870
	sol 2, 5YSZ film	400	1	-0.107	0.029
			3	-0.164	0.039
		600	1	-0.202	1.097
			3	-0.253	2.640
	sol 3, 7YSZ film	400	1	-0.155	0.025
			3	-0.133	0.018
		600	1	-0.198	0.536
			3	-0.239	3.800

Above presented results clearly showed that corrosion protection of stainless steel can be achieved only with YSZ coatings heat treated at 400 °C. Still, it remains unsolved why three layer

coatings do not provide much higher corrosion protection than one layer coatings. For that reason EIS measurements were conducted in 3.5 *wt*.% NaCl (Figure 7). The impedance modulus at the lowest frequencies of protected samples is one order of magnitude higher than that of the bare steel. Similar to polarization measurements, results of electrochemical impedance spectroscopy indicate that protection given by three layer coating is not superior to that of one layer coating. Obtained EIS spectra were analysed using electrical equivalent circuit models presented in Figure 8.

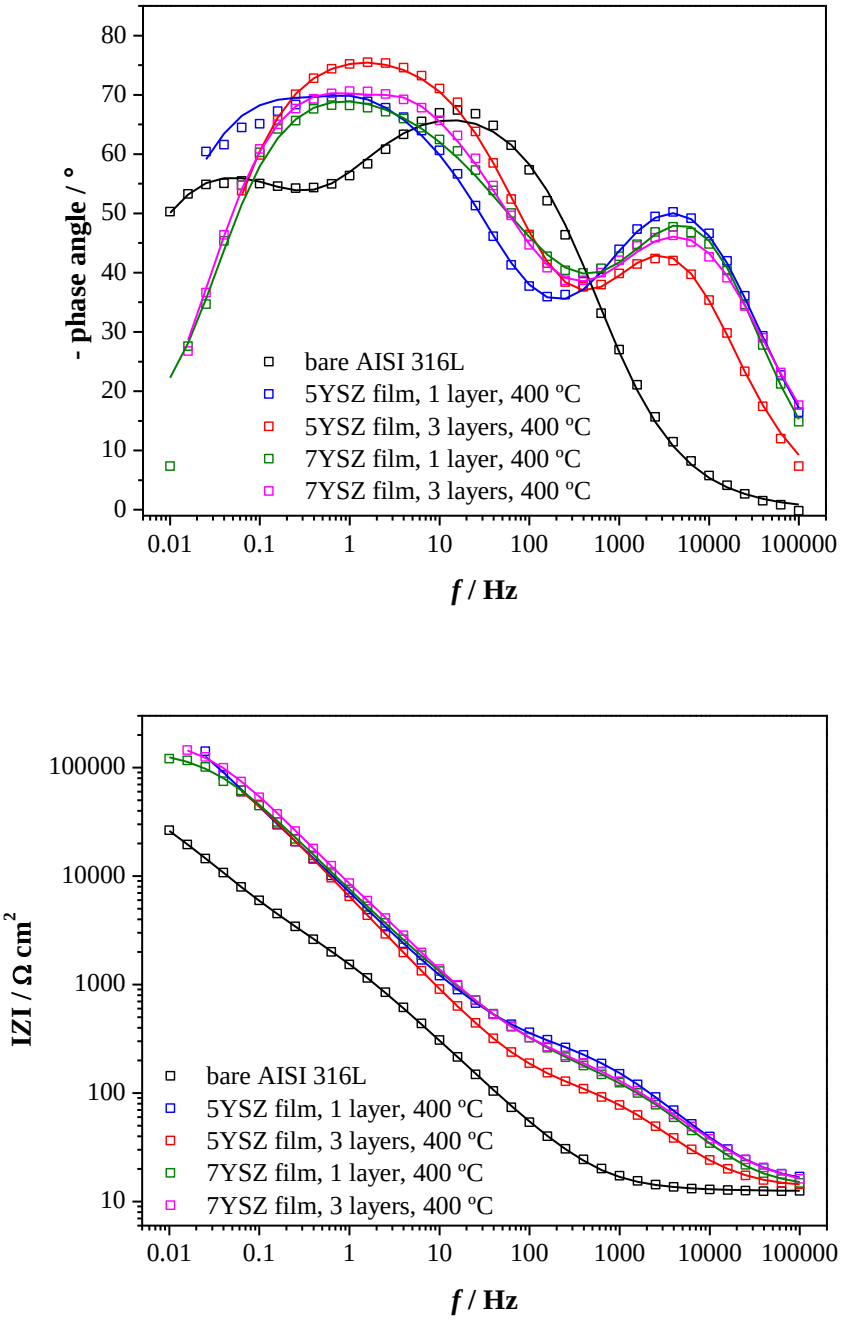

Figure 7. Bode plot for uncoated AISI 316L stainless steel and coated with ZrO_2 films with 1 layer and 3 layers obtained from sol 2 (5YSZ film) and sol 3 (7YSZ film), heat treated at 400 °C for 60 min. Symbols represent experimental data and solid lines fitted data.

From Bode plot of phase angle versus frequency for bare steel two phase angle maxima are easily observed. The one at higher frequencies can be related to the presence of thin oxide layer that is characterized with resistance R_f and capacitance C_f. The second one at lower frequencies can be related to corrosion process occurring at the steel surface and can be represented with the charge transfer resistance R_{ct} and double layer capacitance C_{dl} [25]. However, real systems rarely exhibit ideal capacitive behaviour and for that reason capacitive elements are usually represented by constant phase element CPE [26]. The impedance of CPE is defined as

$$Z(\mathrm{CPE}) = \frac{1}{Q(j\omega)^n} \quad (1)$$

where Q is the constant of the CPE element, j imaginary number, ω is the angular frequency, and n is the CPE exponent where $-1 \leq n \leq 1$. The value of n is associated with the non-uniform distribution of current as a result of roughness and surface defects. The n values of nearly one suggest nearly ideal capacitive behaviour. The value of pseudocapacitance C can be calculated using relationship $C = (QR_b^{1-n})^{1/n}$ according to Brug et al. [27].

The electrical equivalent circuit representing the behaviour of unprotected stainless steel is shown in Figure 8a, where the electrolyte resistance between the working and reference electrodes is represented by R_e. Bode plots of EIS spectra for coated samples also clearly show the presence of two phase angle maxima where the one at the highest frequencies corresponds to processes occurring through pores of the coating and the one at lower frequencies related to corrosion process. The first process can be described with pore resistance of the film R_f and film capacitance C_f while the second one with the charge transfer resistance R_{ct} and double layer capacitance C_{dl} Still, to obtain the good accordance between fitted and experimental data it was necessary to introduce additional elements into the model. For sol 1 coating with one layer it was a Warburg element representing (W) diffusion into the solution, while for other coatings, cotangent-hyperbolic diffusion impedance (O) representing the finite length diffusion inside the pores [15, 28, 29] was introduced. The impedance response for finite length diffusion is:

$$Z_D = \frac{\tanh\left[B(j\omega)^{0.5}\right]}{Y_0(j\omega)^{0.5}} \quad (2)$$

$$\text{where } B = l/\sqrt{D} \quad (3)$$

In this equation l represents pore length and D diffusion coefficient. Such equivalent electrical circuits were also used by Liu et al. [28, 29] to describe behaviour of steel covered by different PVD coatings in 0.5 M NaCl, as well as in our previous paper [15] on corrosion protection of stainless steel with TiO_2 coating.

Impedance parameters obtained by fitting experimental data to selected EEC are given in Table 3.

Coating capacitance is in general considered to follow the Helmholz model [26]:

$$C_f = \frac{\varepsilon\varepsilon_0 A}{d} \quad (4)$$

where ε_0 is the permittivity of vacuum, ε dielectric constant of the coating material, d thickness and A surface area of the coating. Taking in account this equation one would expect that the C_f of 1

layer coatings is three times bigger than that of 3 layer coatings. However, it can be seen that for studied coatings this is not the case.

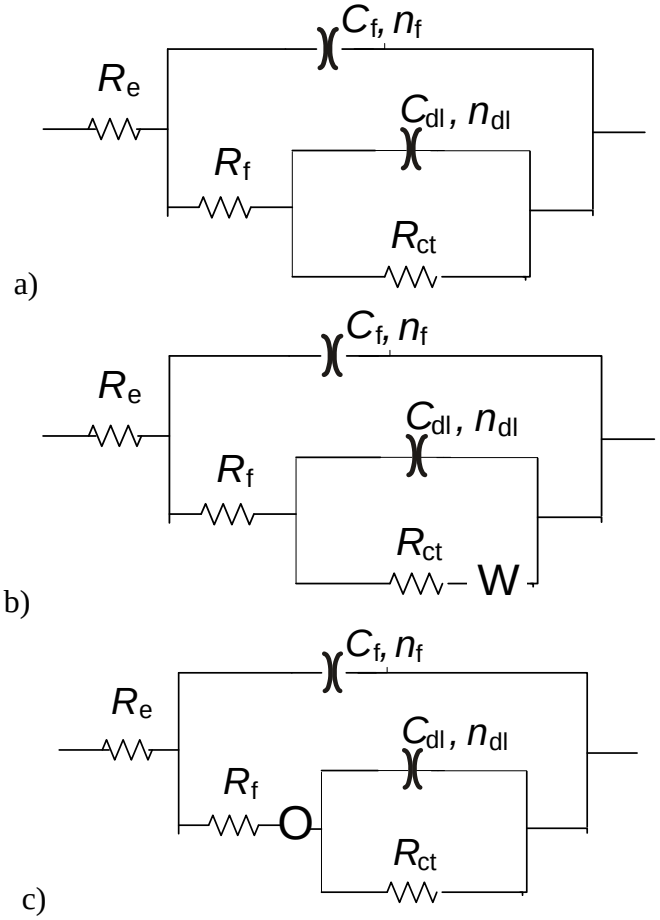

Figure 8. Electrical equivalent circuits used for modelling of experimental EIS data for a) unprotected stainless steel, b) coated with sol 1 (3YSZ film) 1 layer, c) coated with other 1 layer or 3 layers YSZ films.

Table 3. EIS parameters for bare and coated stainless steel AISI 316L determined by fitting experimental data to selected electrical equivalent circuits given in Figure 8 (sol 1: 3YSZ film, sol 2: 5YSZ film and sol 3: 7YSZ film).

Sample	R_f / kΩ cm^2	C_f /μF cm^{-2}	n_f	R_{ct} /kΩ cm^2	C_{dl} / /μF cm^{-2}	n_{dl}
AISI 316L	4.33	103.2	0.79	85.7	429.1	0.73
sol 1, 3YSZ film,1 layer	0.616	0.41	0.88	110	2.89	0.75
sol 1, 3YSZ film, 3 layers	0.108	1.45	0.81	150	37.4	0.91
Sol 2, 5YSZ film, 1 layer	0.307	0.90	0.78	474	4.78	0.83
Sol 2, 5YSZ film, 3 layers	0.184	0.61	0.83	760	25.7	0.87
Sol 3, 7YSZ film, 1 layer	0.163	0.82	0.82	140	36.9	0.85
Sol 3, 7YSZ film, 3 layers	0.217	0.95	0.91	187	20.2	0.91

This can be explained by assuming that water penetrates into the cracks and pinholes in the coating thus increasing dielectric constant of the coating. In other words thicker coatings exhibit bigger number of defects compared to 1 layer coating. This assumption can be also supported by the fact that R_f value does not increase with increase of number of layers (except slightly for sol 3). Formation of cracks within thicker coatings has also been observed by other authors [30]. Still, slightly higher R_{ct} values are observed for thicker coatings such that the thickness of the coating gives certain contribution to overall corrosion protection. From EIS measurements it appears that sol 2 has better protective properties than sol 3, while from polarization measurements inverse conclusion was drawn. This discrepancy might be related to differences in measurements conditions (i.e. potential range) for both methods. It should also be taken in account that Tafel extrapolation method is valid for activation controlled processes, while in our experiments diffusion might also influence corrosion reactions, which can bring an error in performed calculations. However, both methods point out conclusion that sol 1 with the lowest content of Y_2O_3 provides the least efficient protection.

4. CONCLUSIONS

Nanostructured sol-gel ZrO_2 films containing 3 mol % Y_2O_3 (3YSZ film), 5 mol % Y_2O_3 (5YSZ film) and 7 mol % Y_2O_3 (7YSZ film) of one and three layers were deposited on stainless steel X2CrNiMo17-12-2 (AISI 316L) substrate by dip coating method.

Deposited sol-gel ZrO_2 films after calcination at 400 °C and 600 °C were characterized by GD-OES, XRD and electrochemical measurements.

Thickness of ZrO_2 films with 1 layer and 3 layers increase with increasing number of layers and sintering temperature.

Samples treated at lower temperatures and with higher yttria content show finer crystallites, lower porosity and exhibit better corrosion resistance.

The results of electrochemical tests showed that the sol-gel ZrO_2 films sintered at 400 °C, significantly improved the corrosion resistance of austenitic stainless steel X2CrNiMo17-12-2 (AISI 316L) in 3.5 *w*t. % NaCl aqueous solution.

References

1. C.C. Shih, C.M. Shih, Y.Y. Su, L.H.J. Su, M.S. Chang, S.J. Lin, *Corros. Sci.,* 46 (2004) 427.
2. G. Ruhi, O.P. Modi, I.B. Singh, *Corros. Sci.,* 51 (2009) 3057.
3. V. S Saji, R. Cook, Corrosion protection and control using nanomaterials, Woodhead Publishing Limited, 2012, Cambridge, UK.
4. V.S. Saji, J. Thomas, Nanomaterials for corrosion control, *Curr. Sci.*, 92 (2007) 51.
5. S. Sathiyanarayanan, G. Rajagopal, N. Palaniswamy, M. Raghavan, *A review, Corros. Rev.,* 23 (2005) 355.
6. M. Brunet, H. Mafhoz Kotb, L. Bouscayrol, E. Scheid, M. Andrieux, C. Legros, S. Schamm-Chardon, *Thin Solid Films,* 519 (2011) 5638.
7. C. Giolli, F. Borgioli, A. Credi, A.D. Fabio, A. Fossati, M.M. Miranda, S. Parmeggiani, G. Rizzi, A. Scrivani, S. Troglio, A. Tolstoguzov, A. Zoppi, U. Bardi, *Surf. Coat. Technol.,* 202 (2007) 13.

8. D.Q. Peng, X.D. Bai, B.S. Chen, *Surf. Coat. Technol.*, 190 (2005) 440.
9. I. Espitia-Cabrera, H. Orozo-Hernandez, R. Torres-Sanchez, M.E. Contreras-Garcia, P. Bartolo-Perez, L. Martinez, *Mater. Lett.*, 58 (2003) 191.
10. L. Fedrizzi, F.J. Rodriguez, S. Rossi, F. Deflorian, R. Di Maggio, *Electrochim. Acta*, 46 (2001) 3715.
11. W. Xue, Q. Zhu, Q. Jin, and M. Hua, *Mater. Chem. Phys.*, 120 (2010) 656.
12. T. L. Metroke, R. L. Parkhill, E. T. Knobbe, *Prog. Org. Coat.*, 41 (2001) 233.
13. R. Gheriani, R. Chtourou, *J. Nano Res.*, 16 (2012) 105.
14. D. Wang, G.P. Bierwagen, *Prog. Org. Coat.*, 64 (2009) 327.
15. L. Ćurković, H. Otmačić Ćurković, S. Salopek, M. Majić Renjo, S. Šegota, *Corros. Sci.*, 77 (2013) 176.
16. W. Liu, Y. Chen, C. Ye, and P. Zhang, *Ceram. Int.*, 28 (2002) 349.
17. M. Maeda, *Int. J. Electrochem. Sci.*, 10 (2015) 2988.
18. N. Garg, S. Bera, G. Mangamma, C.R. Das, S. Kamaruddin, S. Velmurugan, *Surf. Coat. Technol.*, 281 (2015) 98.
19. C. Amaya, W. Aperador, J.C. Caicedo, F.J. Espinoza-Beltrán, J. Muñoz-Saldaña, G. Zambrano, P. Prieto, *Corros. Sci.*, 51 (2009) 2994.
20. H.M. Abd El-Lateef, M.M. Khalaf, *Mater. Charact.*, 108 (2015) 29.
21. L. Cadoret, N. Reuge, S. Pannala, M. Syamlal, C. Rossignol, J. Dexpert-Ghys, C. Coufort, B. Caussat, *Powder Technol.*, 190 (2009) 185.
22. J. Bautista-Ruiz, W. Aperador, A. Delgado, M. Díaz-Lagos, *Int. J. Electrochem. Sci.*, 9 (2014) 4144.
23. R. Srinivasan, R.J. Deangelis, G. Ice, B.H. Davis, *J. Mater. Res*. 6 (1991) 1287-1292.
24. S. Heiroth, T. Lippert, A. Wokaun, M. Doebeli, J.L.M. Rupp, B. Scherrer, L.J. Gauckler, *J. Eur. Ceram. Soc.* 30 (2010) 489.
25. L. Freire, M. J. Carmezim, M.G.S. Ferreira, M.F. Montemor, *Electrocim. Acta*, 56 (2011) 5280.
26. J. R. Macdonald, Impedance spectroscopy: Emphasising Solid Materials and Systems, John Wiley & Sons, New York (1987).
27. G.J. Brug, A.L.G. van der Eeden, M. Sluyters-Rehbach, J.H. Sluyters, *J. Electroanal. Chem.* 176, (1984) 275.
28. C. Liu, Q. Bi, A. Leyland, A. Matthews, *Corros. Sci.* 45 (2003) 1243.
29. C. Liu, Q. Bi, A. Leyland, A. Matthews, *Corros. Sci*. 45 (2003) 1257.
30. R. Di Maggio, L. Federizzi, S. Rossi, P. Scardi, *Thin Solid Films*, 286 (1996) 127.